



Filiform corrosion behaviour on machined AA7150 aluminium alloy

Bing LIU^{1,2}, Xiao-rong ZHOU², Xin-xin ZHANG^{2,3}

1. State Key Laboratory of Powder Metallurgy, Central South University, Changsha 410083, China;

2. Corrosion and Protection Centre, School of Materials, the University of Manchester,
Sackville Street, Manchester, M13 9PL, UK;

3. Hubei Key Laboratory of Material Chemistry and Service Failure,
Huazhong University of Science and Technology, Wuhan 430074, China

Received 14 November 2019; accepted 18 June 2020

Abstract: The microstructure and the filiform corrosion behaviour of machined AA7150 aluminium alloy were investigated using scanning and transmission electron microscopies combined with potentiodynamic polarization and filiform corrosion testing, respectively. It is found that the grain refinement, redistribution of alloying elements, and elements segregation at grain boundaries are evident within the near-surface region on the machined AA7150 aluminium alloy. The corrosion susceptibility of machining introduced near-surface deformed layer is significantly improved caused by the modified microstructure associated with severe deformation. Filiform corrosion resistance on the machined surface is obviously decreased, due to the surface roughness associated with machining tracks and the presence of the electrochemically more active near-surface deformed layer introduced by machining.

Key words: aluminium alloy; near-surface deformed layer; machining; filiform corrosion

1 Introduction

AA7150 aluminium alloy, as one of the newly developed alloys within the 7xxx series group, is mainly used as the structural material for aircrafts [1–3]. Machining, widely used in aerospace manufacturing to produce components of specific geometry from thick alloy plates, involves significant frictional force between the tool and the work piece, which, like other high shear strain processes, such as rolling and mechanical grinding, introduces extensive shear strain into the near-surface region of the work piece, resulting in near-surface deformed layers [4–7]. The nano-sized grains [8–11], redistribution of alloying element [12,13], presence of oxides [14,15], and elements segregation at the grain boundaries [16], are formed on such alloys.

For aluminium alloys used in the aerospace industry, the failure of materials caused by corrosion is serious and will lead to significant losses [17]. Since deformed layers typically exist in the near-surface region of the aluminium alloys subjected to thermomechanical processings, where corrosion initiates and starts to propagate, the investigation is of significant importance, regarding the influence of the near-surface deformed layer on the corrosion performance of aluminium alloys used in aerospace industry. The near-surface deformed layer may affect the corrosion behaviour of aluminium alloys used in the aerospace industry, due to various factors including segregation of alloying elements [13,18], increased stored energy caused by residual strain [19], and increased population density of grain boundary [20], etc. For 7xxx series aluminium alloys, redistribution of alloying elements within the near-surface deformed

layer has also been reported [13,18]. It is found that the typical strengthening precipitates $MgZn_2$ are dissolved into the aluminium matrix and subsequential segregation of magnesium and zinc occurs at grain boundaries within the near-surface deformed layer on mechanically polished AA7075-T6 aluminium alloy and machined AA7150 aluminium alloy [13]. Such modification of microstructure within the near-surface deformed layer significantly influences the corrosion resistance of the alloy. LIU et al [13] suggest that the machining introduced near-surface deformed layer on AA7150 aluminium alloy is electrochemically more active than the bulk alloy, and preferential dissolution of the deformed layer occurs during immersion in 3.5 wt.% sodium chloride solution.

Filiform corrosion is a typical form of localized corrosion occurring on the coated products of metallic materials [21]. It is often observed in coated aluminium components in aircrafts, such as the edge of aircraft skin, which will significantly influence the effective protection of the organic coating [22]. It is reported that the presence of near-surface deformed layers can promote the initiation and propagation of filiform corrosion on various aluminium alloys [21,23–25], caused by the fine dispersoids and oxides-decorated fine grains, which are sensitive to filiform corrosion. And the difference on the corrosion potential between the near-surface deformed layer and the bulk alloy furtherly promotes the propagation of the filaments [26].

Given that filiform corrosion is a typical type of corrosion on aircraft [27] and machining is a typical manufacturing operation in aerospace [13], the present study aims at investigating the filiform corrosion behaviour of machined AA7150 aluminium alloy by using potentiodynamic polarization, humidity cabinet testing in order to gain insight into the relationship between the machining introduced near-surface deformed layer and the filiform corrosion susceptibility of AA7150 aluminium alloy.

2 Experimental

AA7150 aluminium alloy (Al–7.90Zn–2.61Mg–1.77Cu–0.12Zr–0.06Fe–0.06Si in wt. %) plates were employed in the present work. The

machining of the plates was conducted by milling in the Airbus Company, with the nominal rotation speed of 4000 r/min and the nominal feed rate of 1000 mm/min. The depth of cut was 1 mm for final surface finish. The cutter employed in the milling operation is 160 mm in diameter. The machined plates were then naturally aged at room temperature for 1 year to stabilize the microstructure of the near-surface region.

Alkaline etching was carried out in order to remove the machining introduced near-surface deformed layer and to expose the bulk alloy for characterization and testing to compare with the as-machined condition. Specimens were immersed in a 10 wt.% sodium hydroxide solution for 60 s at 60 °C, and then desmutted in 30 vol.% nitric acid solution for 30 s before being rinsed in deionized water and being dried with cool air stream.

Potentiodynamic polarization was carried out by immersing the specimens in deaerated 3.5 wt.% sodium chloride solution, where a saturated calomel electrode (SCE) and a platinum electrode were used as reference electrode and counter electrode, respectively. The open circuit potential (OCP) was measured before potentiodynamic polarization for 1 h. The specimen was polarized from –30 mV (vs OCP) to 50 mV (vs OCP), with the scanning rate of 0.1667 mV/s. For filiform corrosion testing, specimens of 10 mm × 10 mm, with machined surface or alkaline etched and desmutted surface, were wire-bar coated with a transparent acrylic lacquer to give coating thicknesses in the range of 15–45 μm. Filiform corrosion testing was carried out in a JOHN GODRICH humidity chamber, with the relative humidity and temperature being approximately 75% and 40 °C, respectively. The specimens were checked every 120 h by optical microscopy to record the development of filiform corrosion.

The surface tomography was measured by interferometry using the Contour GT-K 3D optical microscope. Microstructure characterization was mainly carried out by scanning electron microscopy (SEM) and transmission electron microscopy (TEM). Zeiss Ultra 55 field emission gun scanning electron microscope, JOEL 2000 FXII transmission electron microscope and FEI Tecnai TF30 transmission electron microscope were employed in the current work. Specimens for cross-section observations were prepared using the Leica EM

UC6 ultramicrotomy. The analyses of filiform corrosion under each condition were carried out by using the AutoCAD 2018 software and Photoshop CS4 software.

3 Results

3.1 Observation of machined alloy surface

The surface topographic characterization clearly reveals the surface morphology of the machined AA7150 aluminium alloy, as displayed in Fig. 1. Tracks generated by machining operation are

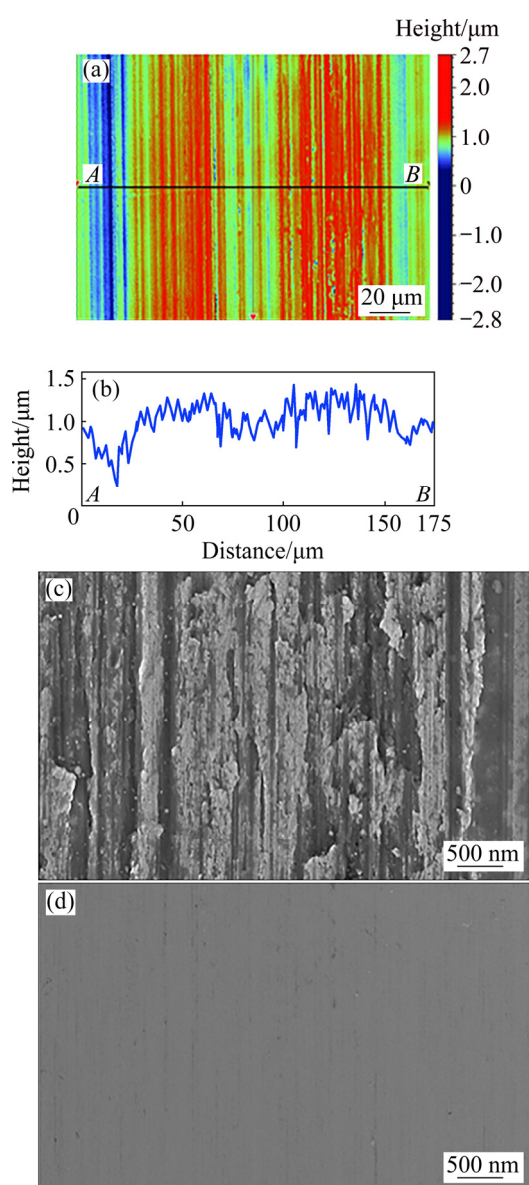


Fig. 1 Surface morphologies of AA7150 aluminium alloy: (a) Contour map by interferometry analysis; (b) Topographic profile along line *AB* indicated in (a); (c) SEM micrograph showing machined surface; (d) SEM micrograph showing as-received surface

mixed with the surface subtle feature, due to possibly worn tool. The surface roughness (R_a) of the alloy is less than $1\ \mu\text{m}$, confirmed from Figs. 1(a) and (b). Since the diameter of the cutter is relatively large compared with the observed region, the machined surface exhibits parallel tracks, as evidenced from Fig. 1(c). However, the as-received alloy exhibits relatively smooth surface, without visible subtle feature, as revealed in Fig. 1(d).

3.2 Microstructure of machined AA7150 aluminium alloy

Figure 2(a) shows the transmission Kikuchi diffraction (TKD) micrograph of the machined AA7150 aluminium alloy. The distribution of the grain orientation within the near-surface region is clearly indicated in the micrograph. A thin layer of 300–500 nm can be observed from the micrograph, which can be clearly distinguished from the underlying region by the nano-sized grains. Figure 2(b) shows TKD micrograph of the dashed line framed region in Fig. 2(a). Grains are less than 100 nm near the alloy surface within the deformed layer, and grain size increases with increasing the depth of the near-surface region up to approximately 500 nm. Large grains are evident in the bulk alloy beneath the near-surface region.

Figure 3(a) shows the micrograph taken on the cross-section of the machined AA7150 aluminium alloy, obtained by high angle annular dark field (HAADF) scanning transmission electron microscopy. A continuous and uniform deformed layer is clearly revealed with the thickness of approximately 300 nm, indicated by the dashed line. Ultrafine equiaxed grains less than 100 nm are present in the deformed layer. Large grains are visible in the bulk alloy region beneath the deformed layer. The distribution of the alloying elements is clearly revealed from the micrograph. Within the near-surface deformed layer, the strengthening precipitates, MgZn_2 , are largely dissolved, and only few particles can be observed, possibly caused by the naturally aging. While the uniform distribution of such precipitates is evident in the bulk alloy with increased population density compared with those in the deformed layer, as indicated by arrows in the micrograph. Furthermore, Fig. 3(b) displays the HAADF micrograph showing the near-surface deformed layer on the machined AA7150 aluminium alloy. The ultrafine grains are

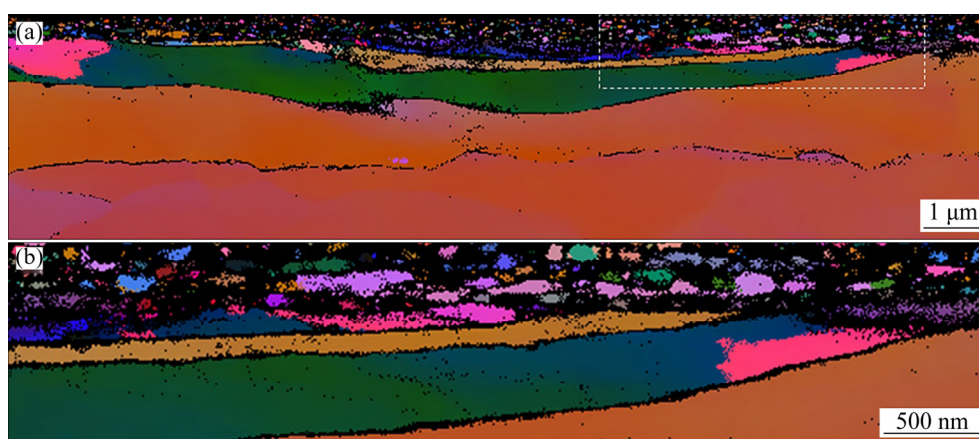


Fig. 2 TKD micrograph showing ultramicrotomed section of machined AA7150 aluminium alloy (a) and region indicated by dashed line frame in (a) at increased magnification (b)

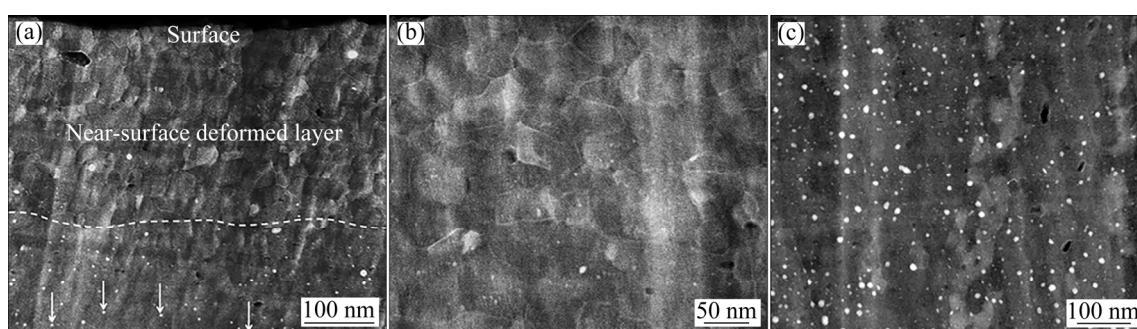


Fig. 3 HAADF micrographs showing ultramicrotomed section of machined AA7150 aluminium alloy (a), near-surface deformed layer (b) and bulk alloy (c)

obvious with bright boundaries, suggesting the elements segregation at the grain boundaries within the near-surface deformed layer. Grains in the deformed layer have diameters less than 100 nm, which are nearly equiaxed. Figure 3(c), the HAADF micrograph revealing the compositional variation of the bulk alloy, displays the uniform distribution of the fine strengthening $MgZn_2$ particles in the bulk alloy beneath the near-surface deformed layer. Such fine precipitates have diameters in the range of 5–20 nm, which are almost absent within the near-surface deformed layer of the machined alloy, as evidenced from Figs. 3(a) and (b).

3.3 Potentiodynamic polarization of machined AA7150 aluminium alloy

The corrosion behaviour of the machined AA7150 aluminium alloy was evaluated by potentiodynamic polarization in deaerated 3.5 wt.% sodium chloride solution at ambient temperature. Figure 4 displays the polarization curve of the machined AA7150 aluminium alloy. Initially, the

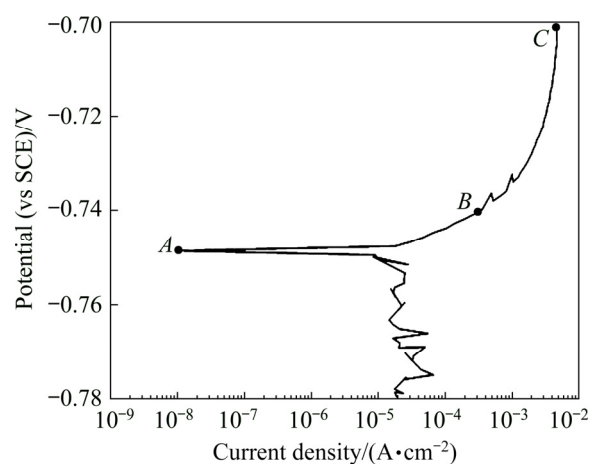


Fig. 4 Potentiodynamic polarization curve of machined AA7150 aluminium alloy in deaerated 3.5 wt.% sodium chloride solution

current density is 1×10^{-5} – 8×10^{-4} A/cm² with slight fluctuations, from -0.78 V (vs SCE) up to the potential approaching to the corrosion potential. Then, it decreases significantly to approximately 1×10^{-8} A/cm², when the potential increases up to the corrosion potential (-0.75 V (vs SCE)). As the

potential gradually increases to -0.70 V (vs SCE), the current density increases dramatically to approximately 0.004 A/cm², and a current surge can be observed.

Three potentials were selected for surface characterization, indicated in Fig. 4 as *A*, *B* and *C*. Figure 5 displays the SEM micrographs showing the testing surface of the machined AA7150 aluminium alloy at different stages after being anodically polarized to the selected potentials in Fig. 4. Potential *A* (-0.75 V (vs SCE)) is the corrosion potential of the machined alloy under the experimental condition, where the anodic and cathodic reactions have achieved a balance, with the current density approaching to zero. The machining

tracks are visible, and the tested alloy surface is intact at this potential, suggesting little evidence of corrosion on the tested alloy surface, as shown in Fig. 5(a). At potential *B*, approximately -0.74 V (vs SCE), where the current density increases dramatically to 3×10^{-4} A/cm², corrosion is clearly revealed within approximately half of the tested surface, as shown in Fig. 5(b). Intact regions are still present with visible machining tracks. The boundary between the corroded region and the intact region is indicated by the dashed line in the micrograph. At potential *C* (-0.70 V (vs SCE)), the attacked regions spread significantly and nearly the entire alloy surface is consumed during the anodic dissolution, as shown in Fig. 5(c).

The anodic dissolution of the alloy was also observed on the cross-section of the alloy after being anodically polarized to potential *B*. The SEM micrograph taken at the location between the corroded and intact regions is displayed in Fig. 6(a). In the corroded region, a thin layer was dissolved immediately beneath the alloy surface. Figure 6(b) exhibits the intact region *A* of the testing alloy in Fig. 6(a) at increased magnification, from which no evidence of corrosion can be observed. According to Fig. 6(c) which exhibits the SEM micrograph showing the corroded region *B* in Fig. 6(a) at increased magnification, it is evident that the corrosion of the alloy was confined within the near-surface deformed layer with the thickness of approximately 300 nm, without further propagation into the bulk alloy. Increased fraction of the deformed layer was anodically dissolved over the current surge in the polarization curve, while the underlying bulk alloy region was intact.

3.4 Filiform corrosion on AA7150 aluminium alloy

Based on the microstructure observation and potentiodynamic polarization of the machined AA7150 aluminium alloy, filiform corrosion of AA7150 aluminium alloy was investigated. It is found that the initiation of filiform corrosion on as-machined surface was first observed at the 15th day. These threadlike filaments initiated at the edge of the as-machined surface covered by the film. Figure 7 illustrates optical micrographs showing the development of filiform corrosion on as-machined surface at the 40th day. Propagation of filiform corrosion was fast on the as-machined surface.

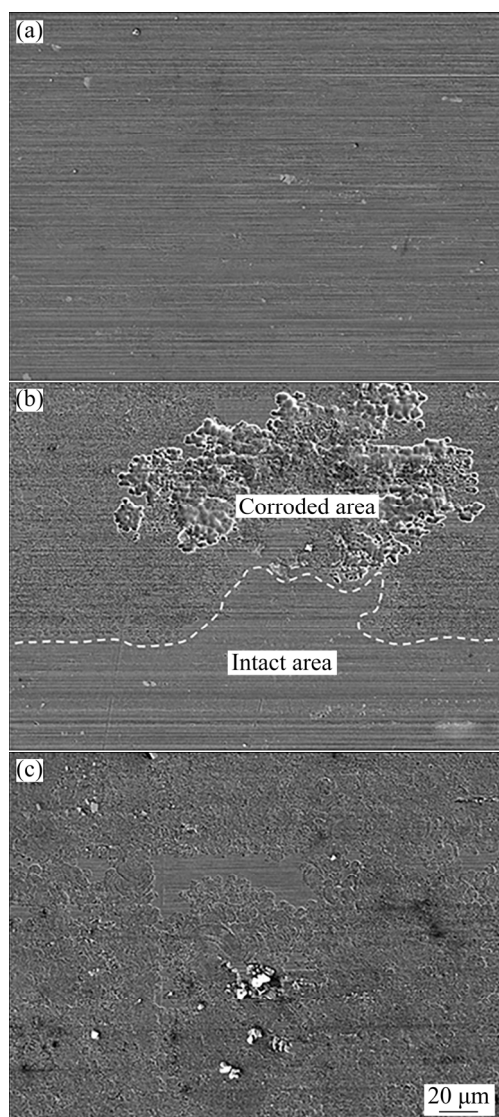


Fig. 5 SEM micrographs showing testing surface of machined AA7150 aluminium alloy at different stages during potentiodynamic polarization indicated in Fig. 4: (a) Potential *A*; (b) Potential *B*; (c) Potential *C*

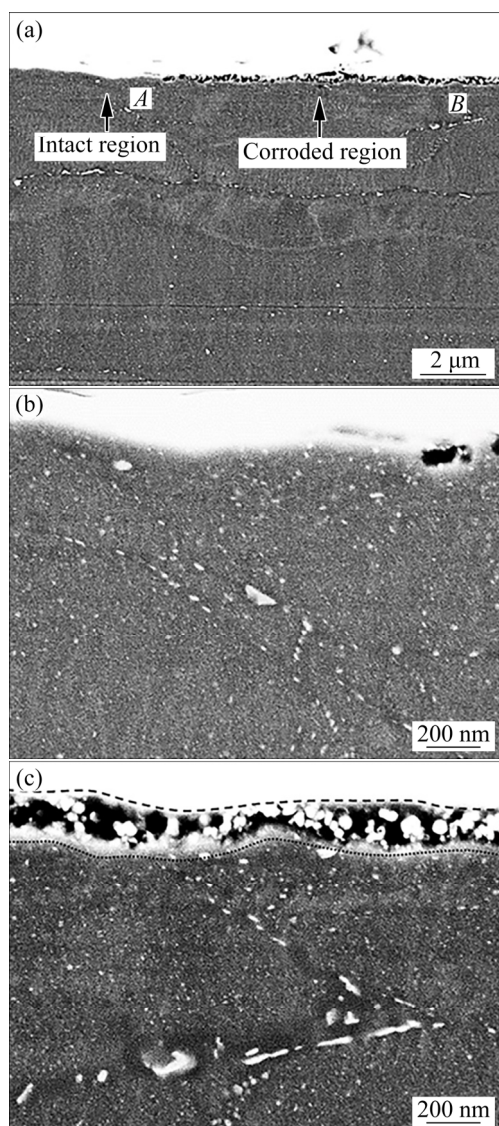


Fig. 6 SEM micrographs showing cross-section of machined AA7150 aluminium alloy at potential *B* during potentiodynamic polarization marked in Fig. 4 (a), intact region *A* in (a) at increased magnification (b) and corroded region *B* in (a) at increased magnification (c)

Filiform corrosion propagated from the edge to the centre of the surface in an irregular shape, and separate initiation sites can be observed. The threadlike filaments are dark grey but regions in black are also revealed with the development of the filiform corrosion, suggesting significant accumulation of the corrosion products [28].

The initiation of filiform corrosion on the etched surface cannot be detected until the 25th day on the edge of the organic film. Figure 8 displays the propagation of filiform corrosion on the etched surface at the 40th day. The threadlike filaments developed slowly, compared with those on the

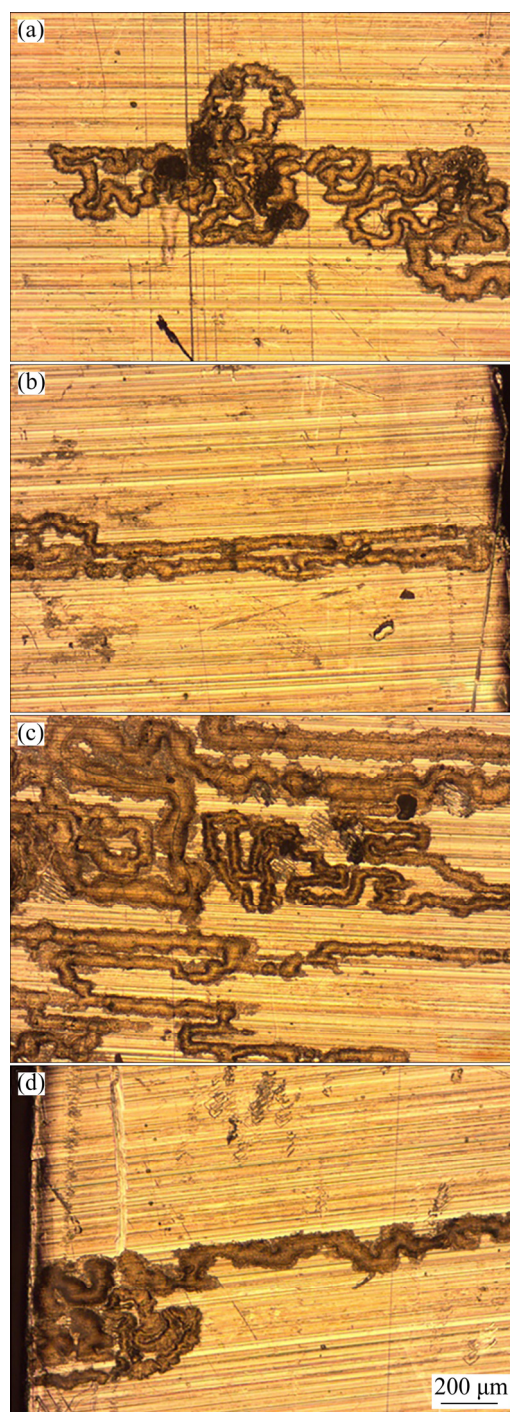


Fig. 7 Optical micrographs of as-machined surface after filiform corrosion testing in humidity cabinet for 40 d, showing initiation and propagation of filiform corrosion: (a, c) Central region; (b, d) Edge

as-machined surface, indicated by arrows in Fig. 8. Such filaments are dark grey, propagating following an irregular pattern. Little evidence of separate initiation was found on the etched surface.

The comparison on the filiform corrosion performance of as-machined and etched AA7150

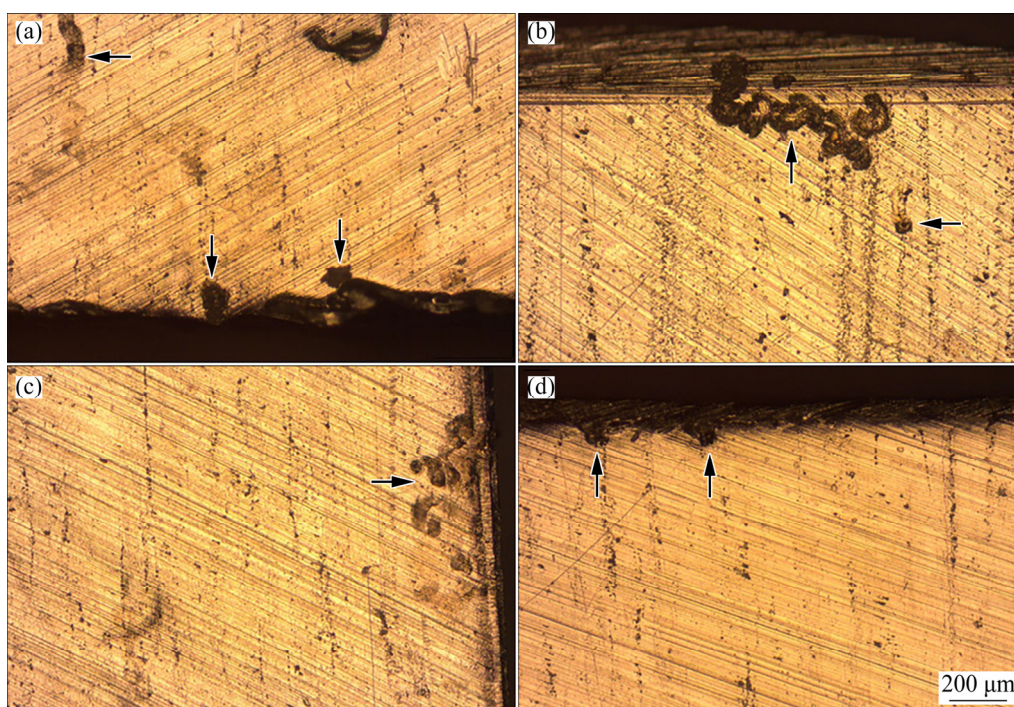


Fig. 8 Optical micrographs of alkaline-etched surface after filiform corrosion testing in humidity cabinet for 40 d, showing initiation and propagation of filiform corrosion: (a) Central region and edge; (b–d) Edge

aluminium alloys is summarized in Table 1. It is revealed that the area fraction with filaments is $(3.00 \pm 0.02)\%$ on the as-machined surface with the presence of the near-surface deformed layer. However, the area fraction of filaments on the etched surface is only $(0.164 \pm 0.001)\%$, where the near-surface deformed layer has been removed. The areas attacked by filiform corrosion are significantly larger on the as-machined surface compared with those on the etched surface.

Table 1 Comparison of filiform corrosion performance of as-machined and alkaline-etched AA7150 aluminium alloys

Parameter	As-machined	Etched
Area fraction with filaments/%	3.00 ± 0.02	0.164 ± 0.001
Number of corrosion sites per unit area/ mm^{-2}	0.27	0.11
Maximum length of filaments/ μm	6118.05 ± 4.87	489.16 ± 1.32
Mean length of filaments/ μm	1830.36 ± 2.01	218.30 ± 0.77

Apparently from Table 1, the number of corrosion sites per unit area is 0.27 mm^{-2} for the as-machined surface and 0.11 mm^{-2} for the etched

surface. On the as-machined surface, the maximum length and the mean length of the filaments are (6118.05 ± 4.87) and $(1830.36 \pm 2.01) \mu\text{m}$, respectively. On the etched surface, the maximum length of the filaments is $(489.16 \pm 1.32) \mu\text{m}$, and the mean length is $(218.30 \pm 0.77) \mu\text{m}$. Filiform corrosion on the as-machined surface develops more rapidly, with extremely longer filaments.

4 Discussion

According to the observation on the deformed layer and the bulk region of the machined AA7150 aluminium alloy, it is obvious that the microstructure of the near-surface region has been significantly modified during the machining operation. Severe deformation combined with the elevated temperature during deformation leads to grain refinement, redistribution of alloying elements, as well as dissolution of the strengthening particles. The modification of microstructure of the near-surface region significantly influences the corrosion performance of the machined alloy.

4.1 Corrosion susceptibility of near-surface deformed layer

At the corrosion potential in the polarization

curve (Fig. 4), the anodic and cathodic reactions have reached the same rate with opposite direction of current flow, thus the current density is approaching to zero. At the potentials below the corrosion potential, anodic reaction is largely restricted due to the negative overpotential, and oxygen reduction, i.e. the cathodic reaction, is overwhelming under such a condition. At the potentials above the corrosion potential (-0.75 V (vs SCE)), the anodic reaction is promoted due to the positive overpotential, whereas cathodic reaction is significantly inhibited. Dissolution of the near-surface deformed layer occurs at this stage, as indicated by the rapid increase of current density over the potential range of -0.75 to -0.74 V (vs SCE) in Fig. 4. Then, as the fraction of the deformed layer on the tested surface diminishes dramatically, current density increases slowly and finally stops increasing at -0.70 V (vs SCE).

The examination of the alloy surface and cross-section (Figs. 5 and 6) during the potentiodynamic polarization further confirms that the current surge is closely associated with the fast anodic dissolution of the deformed layer, and corrosion will not penetrate into the bulk alloy before such deformed layer is consumed. Potentiodynamic polarization of the machined AA7150 aluminium alloy clearly suggests an increased corrosion susceptibility of the near-surface deformed layer, compared with the bulk alloy. As introduced, the modification of microstructure within the near-surface deformed layer is evident, including the formation of ultrafine grains, redistribution of alloying elements and segregation of magnesium and zinc at the grain boundaries within the deformed layer. Firstly, the formation of the ultrafine grains introduces increased number of grain boundaries in the near-surface deformed layer. Further, the segregated elements (magnesium and zinc) at the grain boundaries, improve the heterogeneity between the grain boundaries and the grain interior within the deformed layer, leading to higher anodic activity at such locations. Consequently, the boundaries of those ultrafine grains were susceptible to being preferentially attacked during corrosion, which significantly decreased the corrosion resistance of the deformed layer. Apart from the impact exerted by the microstructure modification, increased density of dislocations

generated by shear deformation within the deformed layer further led to increased electrochemical activity of the deformed layer [18,19], which, in combination, promoted the corrosion of the deformed layer. Consequently, the corrosion susceptibility of the near-surface deformed layer was significantly improved, compared with that of the bulk alloy. Thus, fast dissolution of the alloy, confined within the near-surface deformed layer, could be observed, which explained the current surge in the polarization curve.

4.2 Filiform corrosion of AA7150 aluminium alloy

Based on the observations of the initiation and propagation of filiform corrosion on the as-machined and the etched surface (Figs. 7 and 8) and the comparison of the filiform corrosion behaviour of the alloy under different conditions (Table 1), filiform corrosion is largely promoted on the as-machined surface with the formation of the near-surface deformed layer, indicated by the increased area with filaments. More corrosion sites can be observed within the testing area on the as-machined surface compared with those on the etched surface. Additionally, increased maximum length and mean length of the filaments are evident on the as-machined surface. While the initiation and the propagation of filiform corrosion are obviously slower on the etched surface with the removal of the deformed layer.

The initiation of filiform corrosion depends on the detachment between the film and the metal substrate, which may take place in the destroyed regions of the film, the locations with higher roughness on the alloy surface, and the pits, where the corrosion products will largely help weaken the adhesion of the film [26,29,30]. Thus, the initiation time is closely related to the condition of the surface. Detachment between the film and the alloy surface is easier on the as-machined surface, since higher roughness is obtained from the desirable geometric shape (the machining tracks) after machining operation, as confirmed from surface topographic characterization in Fig. 1. Additionally, etching resulted in the removal of the intermetallics on the etched surface [31]. In the AA7150 aluminium alloy, such intermetallics are mainly the cathodic constituent particles, such as the

Al–Cu–Fe particles. The presence of such cathodic intermetallics weakened the adhesion of the film since the aluminium around the intermetallics was preferentially dissolved, resulting in the localized corrosion attack and consequently the formation of the corrosion products [32]. Thus, initiation of filiform corrosion was more rapid on the as-machined surface with higher roughness and larger population density of the intermetallic particles, compared with that on the etched surface. Furthermore, the near-surface deformed layer on the as-machined surface was electrochemically more active, confirmed by the potentiodynamic polarization in Section 3.3, and was anodically dissolved at a higher rate once the oxygen concentration cell formed, compared with the bulk alloy region. Consequently, on the as-machined surface the initiation and propagation of filiform corrosion were accelerated.

The initiation of the filiform corrosion at the edge of the organic film can be explained by the difficulty of detachment between the film and the alloy at the central part of the alloy surface at the early stage. When the filament formed at the edge and propagated further into the central region, the adhesion of the film was weakened due to the continuous formation of the corrosion products between the alloy surface and the film [30]. In the area near the filament, the film may also be easily detached from the alloy surface, similar to the condition at the edge of the surface. Oxygen penetration was facilitated, and filiform corrosion may initiate and develop following the mechanism mentioned above [26,28,29]. For the as-machined surface with higher roughness and larger population density of intermetallics, detachment between the film and the alloy surface was promoted [32]. Thus, separate initiation sites close to the existing filament on the as-machined surface can be observed. For the etched surface, although the earliest initiation also took place at the edge of the surface, no separate initiation of filiform corrosion can be observed near the filament, due to the relatively smooth surface condition, combined with fewer intermetallic particles.

As described in Section 4.1, due to the microstructure modification introduced by severe deformation and the increased dislocation density, corrosion susceptibility of the near-surface deformed layer is significantly promoted,

confirmed by the fast dissolution of the near-surface deformed layer during the potentiodynamic polarization. Increased electrochemical activity of such deformed layer combined with the higher roughness of the as-machined surface leads to the more rapid initiation and propagation of the filiform corrosion on the as-machined surface in the presence of the near-surface deformed layer.

5 Conclusions

(1) Machining operation resulted in the formation of the near-surface deformed layer on AA7150 aluminium alloy. The severe shear deformation caused microstructure modification within the near-surface deformed layer, typically characterized by ultrafine grains with dimensions less than 100 nm, redistribution of alloying elements and elements segregation at the grain boundaries.

(2) The microstructure modification and increased dislocation density introduced by severe shear deformation combined with elevated temperature involved in machining operation led to decreased corrosion resistance of the near-surface deformed layer. Fast dissolution of the anodically more active deformed layer can be observed in potentiodynamic polarization, without further propagation to the deep bulk alloy with higher corrosion resistance.

(3) The near-surface deformed layer exhibited higher filiform corrosion susceptibility compared with the bulk alloy. The initiation and propagation of filiform corrosion were greatly promoted on the as-machined surface, due to the increased roughness caused by machining tracks and the electrochemically more active near-surface deformed layer generated during machining.

Acknowledgments

The authors acknowledge the UK Engineering and Physical Sciences Research Council for support of Light FORM Programme Grant (EP/R001715/1). Dr. Bing LIU is also supported by China Postdoctoral Science Foundation under the Postdoctoral International Exchange Program.

References

- [1] ROMETSCH P A, ZHANG Y, KNIGHT S. Heat treatment

- of 7xxx series aluminium alloys—Some recent developments [J]. Transactions of Nonferrous Metals Society of China, 2014, 24: 2003–2017.
- [2] JACUMASSO S C, OLIVEIRA P H F, MARTINS J P, CARVALHO A L M. Microstructural characterization of interrupted aging on an AA7050 aluminum alloy [J]. Materials Characterization, 2019, 152: 180–187.
- [3] SUN Rui-ji, SUN Qing-qing, XIE Yue-huang, DONG Peng-xuan, CHEN Qi-yuan, CHEN Kang-hua. Enhancing corrosion resistance of 7150 Al alloy using novel three-step aging process [J]. Transactions of Nonferrous Metals Society of China, 2016, 26: 1201–1210.
- [4] FROLISH M F, WALKER J C, JIAO C G, RAITHFORTH W M, BEYNON J H. Formation and structure of a subsurface layer in hot rolled aluminium alloy AA3104 transfer bar [J]. Tribology International, 2005, 38: 1050–1058.
- [5] NIKITIN I, ALTENBERGER I, MAIER H J, SCHOLTES B. Mechanical and thermal stability of mechanically induced near-surface nanostructures [J]. Materials Science and Engineering A, 2005, 403: 318–327.
- [6] CHEN Yan-xia, YANG Yan-qing, FENG Zong-qiang, HUANG Bin, LUO Xian. Surface gradient nanostructures in high speed machined 7055 aluminum alloy [J]. Journal of Alloys and Compounds, 2017, 726: 367–377.
- [7] ZHANG Tao, LU Shi-hong, WU Yun-xin, GONG Hai. Optimization of deformation parameters of dynamic recrystallization for 7055 aluminum alloy by cellular automaton [J]. Transactions of Nonferrous Metals Society of China, 2017, 27: 1327–1337.
- [8] LI Peng-wei, LI Hui-zhong, HUANG Lan, LIANG Xiao-peng, ZHU Ze-xiao. Characterization of hot deformation behavior of AA2014 forging aluminum alloy using processing map [J]. Transactions of Nonferrous Metals Society of China, 2017, 27: 1677–1688.
- [9] PENG Jian, WANG Yong-jian, ZHONG Li-ping, PENG Long-fei, PAN Fu-sheng. Hot deformation behavior of homogenized Al–3.2Mg–0.4Er aluminum alloy [J]. Transactions of Nonferrous Metals Society of China, 2016, 26: 945–955.
- [10] WANG Shan-shan, JIANG Jian-tang, FAN Guo-hua, FRANKEL G S, ZHEN Liang. Effects of long-term natural aging on the altered surface layer on an Al–Zn–Mg–Cu alloy and on corrosion properties [J]. Electrochimica Acta, 2018, 266: 34–42.
- [11] ESTRIN Y, VINOGRADOV A. Extreme grain refinement by severe plastic deformation: A wealth of challenging science [J]. Acta Materialia, 2013, 61: 782–817.
- [12] HUANG Y, ROBSON J D, PRANGNELL P B. The formation of nanograin structures and accelerated room-temperature theta precipitation in a severely deformed Al–4wt.%Cu alloy [J]. Acta Materialia, 2010, 58: 1643–1657.
- [13] LIU Bing, ZHANG Xin-xin, ZHOU Xiao-rong, HASHIMOTO T, WANG Jun-jie. The corrosion behaviour of machined AA7150-T651 aluminium alloy [J]. Corrosion Science, 2017, 126: 265–271.
- [14] FISHER K B, MILLER B D, JOHNS E C, MARQUIS E A. The role of surface deformation in the oxidation response of type 304 SS in high temperature deaerated water [J]. Corrosion Science, 2018, 141: 88–96.
- [15] XIN Long, WANG Zi-hao, LI Jie, LU Yong-hao, SHOJI T. Microstructural characterization of subsurface caused by fretting wear of Inconel 690TT alloy [J]. Materials Characterization, 2016, 115: 32–38.
- [16] LIU Bing, ZHOU Xiao-rong, ZHANG Xin-xin, WANG Jun-jie. Machining introduced microstructure modification in aluminium alloys [J]. Journal of Alloys and Compounds, 2018, 757: 233–238.
- [17] ZHANG Sheng, ZHANG Teng, HE Yu-ting, LIU Dao-xin, WANG Ji-pu, DU Xu, MA Bin-lin. Long-term atmospheric corrosion of aluminum alloy 2024-T4 in coastal environment: Surface and sectional corrosion behavior [J]. Journal of Alloys and Compounds, 2019, 789: 460–471.
- [18] PREMENDRA, CHEN Jiang-hua, TICHELAR F D, TERRY N H, DEWIT J H W, KATGERMAN L. Optical and transmission electron microscopical study of the evolution of surface layer on recycled aluminium along the rolling mills [J]. Surface and Coatings Technology, 2007, 201: 4561–4570.
- [19] ZHANG Xin-xin, ZHOU Xiao-rong, HASHIMOTO T, LINDSAY J, CIUCA O, LUO Chen, SUN Zhi-hua, ZHANG Xiao-yun, TANG Zhi-hui. The influence of grain structure on the corrosion behaviour of 2A97-T3 Al–Cu–Li alloy [J]. Corrosion Science, 2017, 116: 14–21.
- [20] RALSTON K D, BIRBILIS N, DAVIES C H J. Revealing the relationship between grain size and corrosion rate of metals [J]. Scripta Materialia, 2010, 63: 1201–1204.
- [21] AFSETH A, NORDLIEN J H, SCAMANS G M, NISANCIOGLU K. Effect of heat treatment on filiform corrosion of aluminium alloy AA3005 [J]. Corrosion Science, 2001, 43: 2093–2109.
- [22] WANG Chen-guang, CHEN Yue-liang, ZHANG Yong, JI Jing-jing. Simulation study on filiform corrosion of aircraft aluminum alloy/coating system [J]. Development and Application of Materials, 2017, 32: 80–88.
- [23] AFSETH A, NORDLIEN J H, SCAMANS G M, NISANCIOGLU K. Effect of thermo-mechanical processing on filiform corrosion of aluminium alloy AA3005 [J]. Corrosion Science, 2002, 44: 2491–2506.
- [24] AFSETH A, NORDLIEN J H, SCAMANS G M, NISANCIOGLU K. Filiform corrosion of AA3005 aluminium analogue model alloys [J]. Corrosion Science, 2002, 44: 2543–2559.
- [25] LIU Yan-wen, HASHIMOTO T, ZHOU Xiao-rong, THOMPSON G E, SCAMANS G M, RAINFORTH W M, HUNTER J A. Influence of near-surface deformed layers on filiform corrosion of AA3104 aluminium alloy [J]. Surface and Interface Analysis, 2013, 45: 1553–1557.
- [26] MCMURRAY H N, HOLDER A, WILLIAMS G, SCAMANS G M, COLEMAN A J. The kinetics and mechanisms of filiform corrosion on aluminium alloy AA6111 [J]. Electrochimica Acta, 2010, 55: 7843–7852.
- [27] ZHOU Xiao-rong, THOMPSON G E, SCAMANS G M. The influence of surface treatment on filiform corrosion resistance of painted aluminium alloy sheet [J]. Corrosion Science, 2003, 45: 1767–1777.
- [28] SLABAUGH W H, DEJAGER W, HOOVER S E,

- HUTCHINSON L L. Filiform corrosion of aluminum [J]. Journal of Paint Technology, 1972, 44: 76–83.
- [29] VARGEL C, JACQUES M, SCHMIDT M P. Corrosion of aluminium [M]. Amsterdam: Elsevier, 2004.
- [30] NAZAROV A, ROMANO A P, FEDEL M, DEFLORIAN F, THIERRY D, OLIVIER M G. Filiform corrosion of electrocoated aluminium alloy: Role of surface pretreatment [J]. Corrosion Science, 2012, 65: 187–198.
- [31] MA Yan-long, ZHOU Xiao-rong, THOMPSON G E, SKELDON P. Surface texture formed on AA2099 Al–Li–Cu alloy during alkaline etching [J]. Corrosion Science, 2013, 66: 292–299.
- [32] LEBOZEC N, PERSSON D, THIERRY D. In situ studies of the initiation and propagation of filiform corrosion on aluminium [J]. Transactions of the Institute of Metal Finishing, 2003, 23: 111–122.

机加工 AA7150 铝合金的抗丝状腐蚀性能

刘 竝^{1,2}, 周晓融², 张欣欣^{2,3}

1. 中南大学 粉末冶金国家重点实验室, 长沙 410083;
2. Corrosion and Protection Centre, School of Materials, the University of Manchester, Sackville Street, Manchester, M13 9PL, UK;
3. 华中科技大学 材料化学与服役失效湖北省重点实验室, 武汉 430074

摘 要: 采用扫描及透射电子显微技术表征机加工 AA7150 铝合金近表面变形层的显微组织, 并结合动电位极化曲线及丝状腐蚀测试研究机加工后 AA7150 铝合金的丝状腐蚀行为。研究发现, 机加工后 AA7150 铝合金近表面区域出现晶粒细化、合金元素重新分布以及晶界偏析等特征。机加工过程中强烈的塑性变形导致近表面区域显微组织的改变, 从而极大地提高合金近表面变形层的腐蚀倾向。机加工使合金表面粗糙度增大, 并导致形成电化学活性明显提高的近表面变形层。在二者共同影响下, 机加工后 AA7150 铝合金的抗丝状腐蚀性能明显下降。

关键词: 铝合金; 近表面变形层; 机加工; 丝状腐蚀

(Edited by Wei-ping CHEN)